Tailoring the Reactor Properties in the Small-Scale Sorption-Enhanced Methanol Synthesis

Emanuele Moioli* and Tilman Schildhauer

The performance of a fixed-bed and entrained flow reactor for the sorption-enhanced methanol synthesis from CO_2 is assessed by modelling. Both reactors achieve good performance but show possible drawbacks. The fixed bed reactor requires several units working in parallel, while the entrained flow reactor needs a large volume due to the high superficial particle velocity. We propose a new reactor type, which combines a circulating sorbent with a fluidized bed methanol catalyst in bubbling regime. This solution achieves high CO_2 conversion with high space velocity in a continuous manner.

1 Introduction

The tendency towards the cleaner production of base chemicals is currently calling for a rethinking of the chemical synthesis routes, to adapt to the different availability of raw materials. The production of renewable hydrogen follows different pathways than the fossil fuel-based processes, generally operating at different scales. In this sense, it can be envisaged that the small-scale production of base chemicals gains importance with the energy transition [1]. The methanol production is an example of this possible transition towards renewable materials. Methanol is currently produced using CO and H_2 in the standard synthesis process:

$$CO + 2H_2 \rightleftharpoons CH_3OH$$
$$\Delta H_R^0(298\ K) = -91\ \text{kJ mol}^{-1}$$
(1)
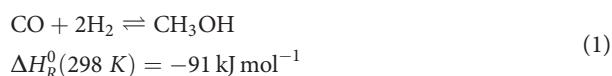
CO and H_2 are generally produced from fossil fuels, for example from natural gas steam reforming [2]. In parallel to the methanol synthesis, over the commercially used $Cu/ZnO/Al_2O_3$ catalyst, the reverse water gas shift reaction (RWGS) occurs, which allows using CO_2 as feedstock [3]. The stoichiometry of the RWSG reaction is:

$$CO_2 + H_2 \rightleftharpoons CO + H_2O$$
$$\Delta H_R^0(298\ K) = 41.5\ \text{kJ mol}^{-1}$$
(2)
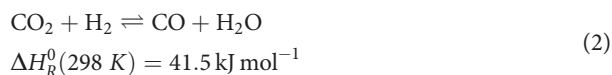
While the standard fossil-based methanol synthesis is performed in continuous large-scale plants, the amount of H_2 produced in renewable-powered electrolysis units is in the MW-scale [4]. Hence, if this resource is used as feedstock, the scale of the chemical reactor should be significantly decreased. In the current processes, the thermodynamic equilibrium is shifted by means of high pressure. The

required compression is obtained at low cost by feeding the hot gases coming from the reforming step to a turbine [2]. This important thermal integration is not anymore available in the renewable methanol production as the synthesis process is decoupled from the natural gas steam reforming step. Hence, the compression cost may become significant in the renewable methanol synthesis, requiring the use of other strategies for the shift of thermodynamic equilibrium [5].

A promising pathway for the enhancement of methanol synthesis is the selective removal of products. This concept was experimentally verified by Westerterp et al. by means of a couple of tubular reactors in series with inter-stage methanol absorption, showing a significant increase in single-pass conversion with this configuration [6]. Following this concept, several studies highlighted the possibility of producing methanol via membrane reactors [7]. The current drawback of this technology is the limitation to rather mild temperature and pressure conditions. Other studies focused on the removal of the products by in situ condensation, showing high reaction yield and shift of the thermodynamic equilibrium [8, 9]. Unfortunately, these reaction concepts also show a significant energy demand to perform the recirculation of reactants. Another option for the selective removal of reaction products is the use of ionic liquids [10].

[1]Dr.-Ing. Emanuele Moioli

https://orcid.org/0000-0002-2943-6823

(Emanuele.moioli@psi.ch), [1]Dr. Tilman Schildhauer

[1]Energy and Environment Division, Paul Scherrer Institute, Forschungsstrasse 111, 5232 Villigen, Switzerland.

In this paper, the focus lies in the assessment of sorption-enhanced techniques for the thermodynamic equilibrium shift in the methanol synthesis. Sorption-enhancement is a well-known technique, which was applied to several reactions, including steam reforming [11], CO_2 methanation [12], water-gas-shift reaction [13] and dimethyl-ether production [14]. Sorption enhanced methanol synthesis was demonstrated in some recent studies using Cu-based catalysts mixed with zeolites, which act as water sorbents [15, 16]. The water adsorption has a double promoting effect on the methanol synthesis. On one hand, the in situ water removal shifts the thermodynamic equilibrium, hence causing an increase in the reaction yield [15]. On the other hand, the water removal prevents the inhibition of catalyst active sites due to competitive adsorption [17]. The selection of the appropriate zeolite for this process is guided by the goal of selectively trapping water molecules. Several studies showed that molecular sieves in the 3 Å range are ideal for applications in the methanol synthesis [18, 19] and will hence be used as a reference material in this study.

Goal of this study is to analyze the possibility of implementing the sorption-enhanced methanol synthesis in technical reactors. This will be performed by comparing the performance of different reactor types in the sorption-enhanced methanol synthesis in terms of space-time yield. Primarily, the performance of a series of dynamic fixed bed reactors is computed to determine the dimension and number of units required to achieve the target methanol productivity. This performance will be compared with the simulation results of an entrained flow reactor. Compared to the former case, the latter reactor requires only one reactor vessel, as catalyst and sorbent are continuously exchanged [20]. However, in the entrained flow reactor, the attainable residence time is rather small, because of the entrainment conditions, which require high superficial gas velocity. After the analysis of pros and cons of these reactor technologies, a new reactor type was proposed. In this equipment, a combination of fluidized bed and entrained flow reactors is realized. This is achieved by selecting the particle size of catalyst and sorbent in a way that the catalyst is kept in suspension in the reactor (fluidized bed) and the sorbent is entrained. In this way, it is possible to achieve a significantly higher residence time of the gas on the catalyst bed, while ensuring a continuous regeneration of the sorbent.

2 Computational Details

2.1 Reactors Analyzed

The details of the three reactor types analyzed are shown in Fig. 1. The dynamic fixed bed reactor is composed of two
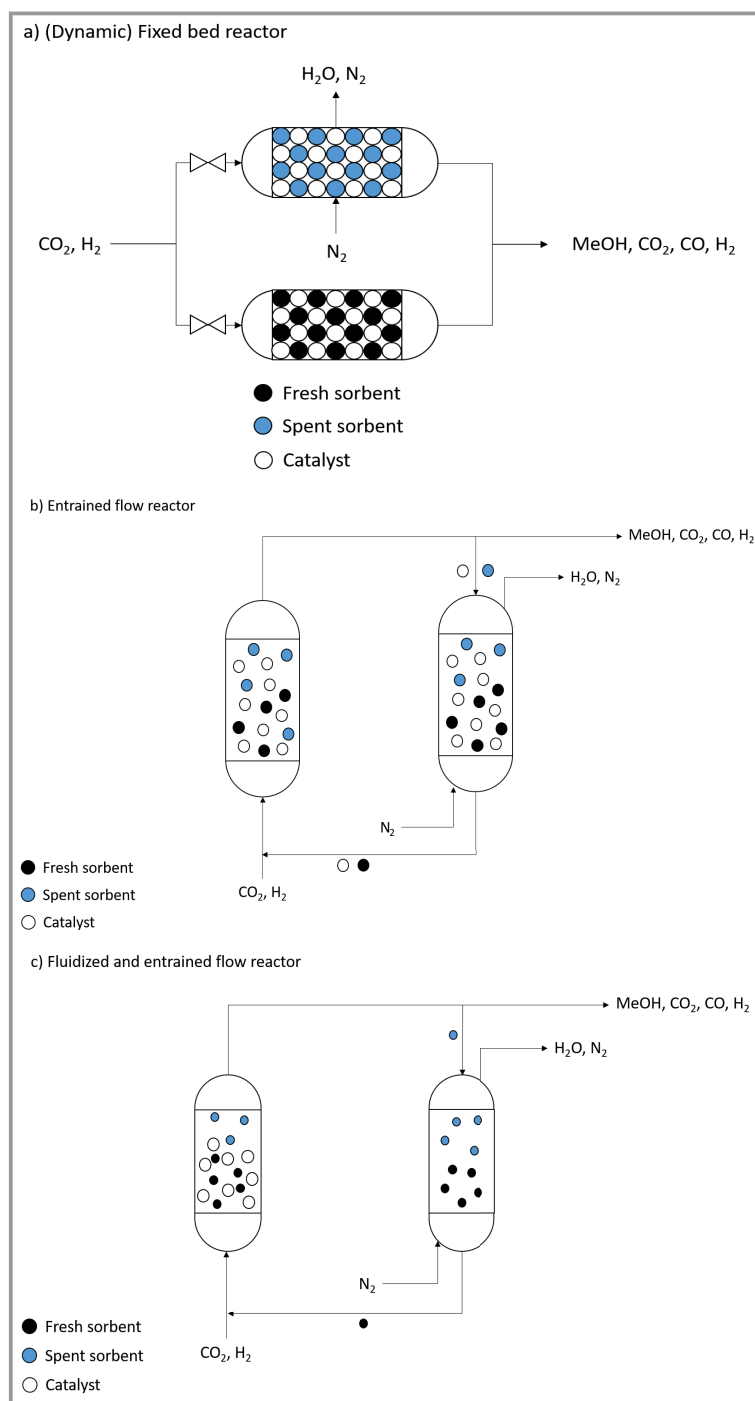

Figure 1. The three reactor types analyzed: a) dynamically operated fixed bed reactor, b) entrained flow reactor, c) fluidized bed (catalyst) and entrained flow (sorbent) reactor.

reactors in parallel, one operated in reaction mode and the other in regeneration mode. The regeneration is operated by feeding an inert gas (e.g., N_2) and by keeping the reactor warm using the waste heat coming from the reactor in reactive mode. The regeneration step is not modelled in detail. The entrained flow reactor is operated by entraining both catalyst and sorbent. When leaving the reactor, the particles are separated from the gas phase and fed to regeneration unit, which is operated with an inert gas and using the waste heat from the methanol reactor. The regenerated sorbent is then fed back, together with the catalyst, to the main reactor. The entrained/fluidized bed reactor generates two different flow patterns in the reactor by using different particle sizes. The catalyst remains in suspension in the reactor (fluidized phase) while the sorbent is sufficiently small to be entrained from the gas. The entrained sorbent is separated from the gas phase and regenerated in analogy to the entrained flow reactor.

2.1.1 Dynamic Fixed Bed Reactor

The dynamic fixed bed reactor has a volume of $20\,m^3$ and is composed of 5000 pipes in parallel with diameter of 0.01 m. Due to the small-scale focus, the reactor diameter considered is slightly smaller than the standardly used reactor diameter, which is in the order of 0.03–0.05 m [21]. The diameter-to-pellet ratio is kept in a safe range to avoid undesired effects. The total feed is $20\,kmol\,h^{-1}$ of a stoichiometric 1:3 CO_2:H_2 gas mixture at 30 bar. The sorbent to catalyst ratio is 1:1. The kinetic model for the methanol synthesis is from Vanden Bussche and Froment [22] and the sorbent model is from Maksimov et al. [16]. The model is as follows:

Mass balance for component i (except H_2O):

$$\frac{\partial y_i}{\partial t} = \frac{\varepsilon_b}{\varepsilon_t} v_0 \frac{\partial p_i}{\partial z} - \frac{\rho_{cat} RT}{\varepsilon_t} \sum_{j=1}^{NR} \eta \nu_{i,j} R_j (1 - \varphi_c) \tag{3}$$

Mass balance for H_2O:

$$\frac{\partial y_{H_2O}}{\partial t} = \frac{\varepsilon_b}{\varepsilon_t} v_0 \frac{\partial p_i}{\partial z} - \frac{\rho_{cat} RT}{\varepsilon_t} \sum_{j=1}^{NR} \eta \nu_{H_2O,j} R_j (1 - \varphi_c)$$
$$- \frac{\rho_{ads} RT}{\varepsilon_t} \frac{\partial q_{H_2O}}{\partial t} \tag{4}$$

Energy balance:

$$\rho_{tot} c_p \frac{\partial T}{\partial t} = \frac{c_p \varepsilon_b}{R} v_0 \frac{\partial T}{\partial z} - \frac{\rho_{cat} RT}{\varepsilon_t} \sum_{j=1}^{NR} \eta R_j \left(-\Delta H_j^R\right)(1 - \varphi_c)$$
$$- \rho_{ads}(-\Delta H_{ads}) \frac{\partial q_{H_2O}}{\partial t} - \frac{2U}{r_{in}}(T - T_w) \tag{5}$$

Water absorption model:

$$\frac{\partial q_{H_2O}}{\partial t} = U\left(q_{H_2O}{}^\star - q_{H_2O}\right) \tag{6}$$

Equilibrium loading of the adsorbent:

$$q_{H_2O}{}^\star = \frac{m_{H_2O} b_{H_2O} p_{H_2O}}{1 + m_{H_2O} p_{H_2O}} \tag{7}$$

For the calculation of the gas velocity, the continuity equation is used. The catalyst efficiency is calculated with the generalized Thiele modulus for a catalyst pellet. The catalyst efficiency factor is calculated via the generalised Thiele modulus:

$$\phi = \frac{V_p}{S_p} \sqrt{\frac{n+1}{2} \left(\frac{k c_{i,s}^{n-1}}{D}\right)} \tag{8}$$

$$\eta = \frac{3}{\phi^2}(\phi \coth(\phi) - 1) \tag{9}$$

The parameters of the system are obtained from [16] and reported in Tab. 1. The model equations are solved in MATLAB by discretizing the space variable with the method of lines (20 points) and by resolving the resulting system of ordinary differential equations with the *ode15s* function.

Table 1. The parameters for the dynamic fixed bed reactor (elaborated from [16]).

Parameter	Value
Bed porosity ε_b [–]	0.34
Total porosity ε_t [–]	0.52
Catalyst density ρ_{cat} [kg m^{-3}]	1450
Catalyst fraction φ_{cat} [–]	0.5
Heat of water adsorption ΔH_{ads} [kJ mol^{-1}]	78
Langmuir adsorption parameter for water adsorption* $b_{H_2O,0}$ [–]	$1.04 \cdot 10^{-15}$

*The water adsorption parameter is calculated according to the Langmuir isotherm $b_{H_2O} = b_{H_2O,0} \exp\left(-\frac{\Delta H_{ads}}{RT}\right)$.

2.1.2 Entrained Flow Reactor

The entrained flow reactor is simulated with a 1D model, assuming steady-state conditions, negligible axial and radial dispersion and uniform water adsorption following the formulation in [20]. The intraphase limitations are considered via the Thiele modulus. The superficial velocity of the gas is $0.3\,m\,s^{-1}$. The particles diameter is 0.00003 m. The reactor diameter is 1.5 m and the length is 7 m (reference case).

This corresponds to a flow rate of 80 kmol h^{-1} in the reference case. The material balances are expressed as:

$$\frac{dF_i}{dz} = (1 - \varphi_c)\rho_s\varepsilon_{sd}AH\sum_{j=1}^{NR}\eta\nu_{I,j}R_j \tag{10}$$

The water balance is expressed as:

$$\frac{dF_{H_2O}}{dz} = (1 - \varphi_c)\rho_s\varepsilon_{sd}AH\sum_{j=1}^{NR}\eta\nu_{H_2O,j}R_j - \varphi_c\varepsilon_{sd}AG_sq_{H_2O} \tag{11}$$

The energy balance is:

$$\sum_{i=1}^{NS}F_ic_{p,i}\frac{dT}{dz} = (1 - \varphi_c)\rho_s\varepsilon_{sd}AH\sum_{j=1}^{NR}\eta\nu_{I,j}R_j - U\pi D$$
$$\times (T - T_w)H \tag{12}$$

The solid circulating rate (G_s) is given by:

$$G_s = U_S^0\rho_s \tag{13}$$

U_S^0 is the superficial solids velocity. The momentum balance is written assuming negligible gas gravity, wall friction and gas velocity variation. Under these assumptions, the balance results in the formula [23]:

$$(-\Delta P)_{dense\ bed} = g\rho_s\varepsilon_{sd}H + \rho_sU_g\varepsilon_{sd}U_t \tag{14}$$

U_g is the gas velocity in the dense region, expressed as:

$$U_g = \frac{U_g^0}{1 + \varepsilon_{sd}} \tag{15}$$

U_g^0 is the superficial gas velocity. ε_{sd} can be calculated by assuming that a critical holdup value exists after which the solids holdup becomes independent from the superficial gas velocity (dense region filling the entire riser). Hence, ε_{sd} is calculated as [24]:

$$\frac{\varepsilon_{sd}}{\varepsilon_s'} = 1 + 6.14\times10^{-3}\left(\frac{U_g^0}{U_s^0}\right)^{-0.23}\left(\frac{\rho_s - \rho_g}{\rho_g}\right)^{1.21}\left(\frac{U_g^0}{\sqrt{gD}}\right)^{-0.383}$$

$$\text{for}\quad G_s < G_s^* \tag{16}$$

$$\frac{\varepsilon_{sd}}{\varepsilon_s'} = 1 + 0.103\left(\frac{U_g^0}{U_s^0}\right)^{1.13}\left(\frac{\rho_s - \rho_g}{\rho_g}\right)^{-0.013}\quad\text{for}\quad G_s \geq G_s^* \tag{17}$$

ε_s' is the solids holdup when the slip velocity equals U_t:

$$\varepsilon_s' = \frac{G_s}{\rho_s\left(U_g^0 - U_t\right)} \tag{18}$$

The saturation carrying capacity is expressed as [25]:

$$\frac{G_s^*d_s}{\mu_g} = 0.125Fr^{1.85}Ar^{0.63}\left(\frac{\rho_s - \rho_g}{\rho_g}\right)^{-0.44} \tag{19}$$

The Froude (Fr) number is expressed as:

$$Fr = \frac{U_g^0}{\sqrt{gD}} \tag{20}$$

The Archimedes (Ar) number is calculated as:

$$Ar = \frac{d_s^3\rho_gg\left(\rho_s - \rho_g\right)}{\mu_g^2} \tag{21}$$

The particle terminal velocity (U_t) is obtained by calculating the dimensionless terminal velocity (U_t^*) and the dimensionless particle diameter (d_s^*) as follows [26]:

$$U_t^\star = \left(\frac{18}{d_s^{*2}} + \frac{2.3348 - 1.7439\ \phi_P}{d_s^{*0.5}}\right)^{-1} \tag{22}$$

$$d_s^\star = \left(\frac{3}{4}C_DRe^2\right)^{1/3} = d_s\left(\frac{g\rho_g\left(\rho_s - \rho_g\right)}{\mu_g^2}\right)^{1/3} \tag{23}$$

$$U_t = U_t^*\left(\frac{g\mu_g\left(\rho_s - \rho_g\right)}{\rho_g^2}\right)^{1/3} \tag{24}$$

ϕ_P is the sphericity of the particles, Re is the Reynolds number:

$$Re = \frac{d_sU_t\rho_g}{\mu_g} \tag{25}$$

C_D is the drag coefficient, expressed as:

$$C_D = \frac{4}{3}\frac{gd_s}{U_t^2}\left(\frac{\rho_s - \rho_g}{\rho_g}\right) \tag{26}$$

The system of differential equations resulting from the model is implemented in MATLAB and solved with the function *ode23t*.

2.1.3 Fluidized and Entrained Flow Reactor

The fluidized and entrained flow reactor is simulated with a modified two-phase reactor model [27]. The reactor has a diameter of 1.5 m and a length of 2 m. The sorbent has a diameter of 0.0003 m, while the catalyst has a diameter of 0.0015 m. The model consists of the bubble phase and two dense phases: one canonical fluidized phase (catalyst in

bubbling regime) and one entrained phase (sorbent in circulating regime). In the canonical fluidized phase, the main reactions take place, while in the entrained phase only the water adsorption occurs. The main assumptions of this model are similar to the previous cases: steady-state conditions, plug flow behavior of the bubble phase, the dense phase is well mixed, interphase and intraparticle diffusion resistances are negligible due to small catalyst particles. The resulting model equation are:

Mass balance on the main components (bubble phase):

$$\frac{dF_{ib}}{dh} = -(K_{bd})_{ib}\left(\frac{F_{ib}}{Q_b} - \frac{F_{id}}{Q_d}\right)A_b \tag{27}$$

The mass balance of water contains an additional term of adsorption on the entrained sorbent particles:

$$\frac{dF_{H_2O,b}}{dh} = -(K_{bd})_{ib}\left(\frac{F_{ib}}{Q_b} - \frac{F_{id}}{Q_d}\right)A_b - \varphi_c\varepsilon_{sd}AG_sq_{H_2O} \tag{28}$$

The energy balance is:

$$\frac{dT_b}{dh} = \frac{(H_{bd})_bA_b(T_d - T_b) - \varphi_c\varepsilon_{sd}AG_sq_{H_2O}\Delta H_{ads}}{\rho_gC_{pg}Q_b} \tag{29}$$

The mass balance of the dense phase is:

$$F_{id} = (F_{id})_F + \int_0^H (K_{bd})_{ib}\left(\frac{F_{ib}}{Q_b} - \frac{F_{id}}{Q_d}\right)A_b dh + V$$

$$\times (1-\delta)(1-\varepsilon_{mf})\rho_s\sum_{j=1}^{NR}\nu_{ij}R_j \tag{30}$$

The energy balance of the dense phase is:

$$\rho_gC_{pg}Q_d(T_F - T_{ref}) - \rho_gC_{pg}Q_d(T_d - T_{ref})$$

$$- \int_0^H (H_{bd})_bA_b(T_d - T_b)dh + V(1-\delta)(1-\varepsilon_{mf})\rho_s\sum_{j=1}^{NR}\Delta H_jR_j$$

$$- U\pi D(T_d - T_W) = 0 \tag{31}$$

The hydrodynamic parameters are reported in appendix. The model equations are implemented in MATLAB and solved with the function *ode23t*.

2.2 Comparison Parameters

The comparison of the reactors is made according to the following parameters:
CO$_2$ conversion:

$$X_{CO2} = \frac{F_{CO2}^0 - F_{CO2}^{out}}{F_{CO2}^0} \tag{32}$$

Methane yield:

$$Y_{MeOH} = \frac{F_{MeOH}^{out}}{F_{CO2}^0} \tag{33}$$

CO yield:

$$Y_{CO} = \frac{F_{CO}^{out}}{F_{CO2}^0} \tag{34}$$

Space velocity:

$$GHSV = \frac{F_{tot}\left[\frac{Nm^3}{h}\right]}{V_{react}[m^3]} \tag{35}$$

To compare a system that is intrinsically discontinuous (dynamic fixed bed reactor) with continuous systems, the conversion and yield indicators of the dynamic fixed bed reactor are averaged over the entire time on stream, i.e., from time = 0 when the sorbent is fresh to the selected time of switch between reactors. The volume of the fixed-bed reactor includes two catalyst-filled units, one in reaction and one in regeneration mode.

3 Results and Discussion

The sorption-enhanced reactions are intrinsically discontinuous operations, as water is adsorbed on the surface of the sorbent material until saturation. Once saturated, the material should be regenerated either in situ or ex situ to remove the water and restore the sorption capacity. The analyzed processes, fixed and entrained flow reactors, differ for the regeneration strategy. In the former case, two identical reactors are operated alternatively in reaction or regeneration. Hence, the regeneration is performed in situ and only one reactor at a time is active in the reaction. In the latter case, the regeneration is performed ex situ and the spent sorbent is continuously removed from the reactor and replaced by fresh catalyst. In the following, the two strategies are analyzed in detail and compared.

3.1 Fixed Bed Reactor

The fixed bed reactor is operated dynamically. Hence, the model used considers the variation of the axial concentration and temperature profile over time. The calculated methanol yield and temperature profiles are shown in Fig. 2. The results are in good agreement with the experimental results reported in [16]. In the first part of the reactor, the reaction is fast, until reaching a value of approximately 25 % methanol yield. This section corresponds to the reaction hotspot area, as visible from the temperature profile. The calculated position and extension of the hotspot is in line with what experimentally reported for the standard
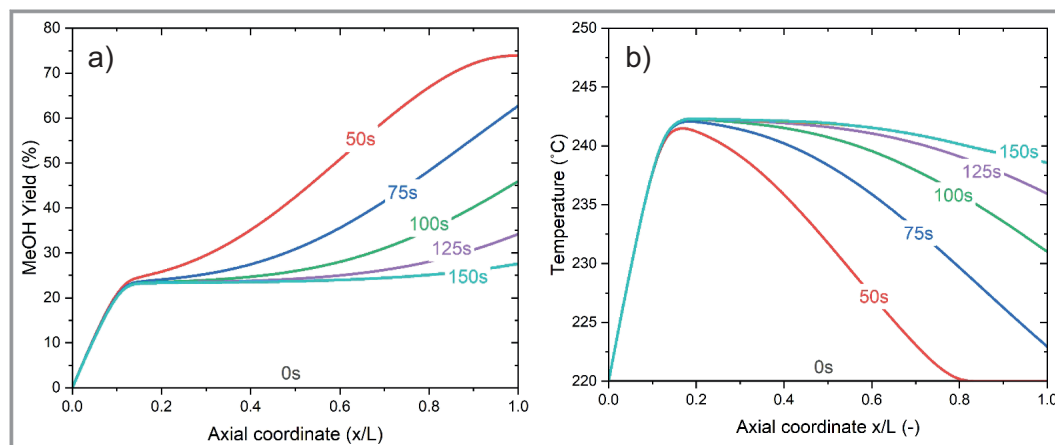
Figure 2. Results of the simulations for the dynamic fixed bed reactor. a) Methanol yield profile, b) temperature profile ($P = 30$ bar, coolant temperature = 220 °C, sorbent/catalyst ratio = 1/1).

CO_2 to methanol reaction [28]. After this first section, the sorption enhancement effect becomes evident. Initially (50 s line), the yield profile increases strongly with the axial coordinate, because the sorbent capacity is high. With the progressive saturation of the sorbent, the profile tends to become flatter, until approximating the standard (non-enhanced) methanol synthesis reaction for a time on stream longer than 150 s. This time span is in line with the switch time of pressure swing adsorption units of industrial relevance [29, 30].

The shift of the water sorption profile is evident in the temperature profile. Initially, most of the water adsorption (exothermic reaction) takes place in the first half of the reactor, so that the heat production in the second half of the reactor is limited. In this way, the cooling is sufficient to reduce the temperature in the second half of the reactor, originating a characteristic hotspot profile. With the proceeding of the reaction, more heat production takes place in the second part of the reactor, as the sorbent in the first part is already saturated. In this way, the heat production is distributed in the entire reactor, increasing the temperature also in the second half of the reactor. The observed profile is hence the result of two different reaction zones: initially, the heat production is controlled by the (fast) methanol synthesis reaction; when the CO_2 conversion approaches the equilibrium value, the water sorption becomes determining, limiting the conversion to the value allowed by the thermodynamic shift. At the same time, water sorption influences the extent of the RWGS reaction, with higher amount of CO present at the reactor outlet with increasing time-on-stream. This suggests that the reactor optimization depends on the adaptation of the relative ratio of catalyst and sorbent, matching the reaction rate and the thermodynamic shift by water removal. This is particularly important when increasing the pressure. In this case, the reaction yield increases, hence causing an increase in the water production. As the water adsorption is an exothermic reaction, the increase in pressure causes an increase in the outlet temper-

ature, as shown in Fig. 3. This in turn causes a decrease in the maximum methanol yield reachable, as a higher temperature implies a lower equilibrium yield. Hence, unless the heat transfer is significantly increased, the increase of pressure has a limited effect on the reaction yield. For these reasons, the sorption-enhanced methanol synthesis is particularly suitable for small-scale applications, where low pressure is required due to the economic impact of compression on the process performance [31].
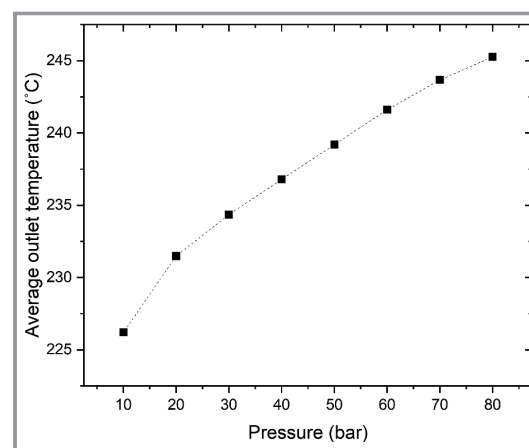

Figure 3. Average outlet temperature in the sorption-enhanced methanol synthesis in the dynamic fixed bed reactor as a function of pressure (coolant temperature = 220 °C, sorbent/catalyst ratio = 1/1, time on stream = 150 s).

The results elucidated in this section confirm that the sorption enhanced methanol synthesis is feasible in fixed bed reactors, but also showed that the management of the dynamic reactor may be challenging, as the complex interplay of reaction, water adsorption and heat transfer should be controlled with care.

3.2 Entrained Flow Reactor

In the entrained flow reactor, the catalyst and sorbent particles are designed to be entrained by the gas flow. Hence, the residence time of the particles in the reactor is limited and the sorbent does not reach the saturation conditions before leaving the reactor. The sorbent:catalyst ratio investigated is 1:1. The results of the simulations for this reactor type are displayed in Fig. 4.
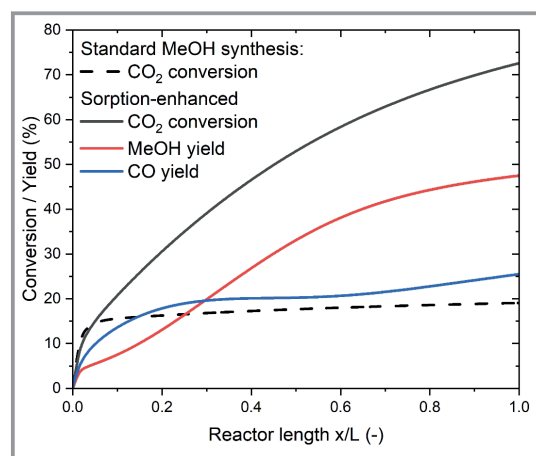

Figure 4. Results of the simulations for the entrained flow reactor, comparing the sorption-enhanced and the standard methanol synthesis ($P = 30$ bar, coolant temperature = 220 °C, sorbent/catalyst ratio = 1/1).

The sorption-enhancement effect is already visible after the first 10 % of the reactor. Initially, the water removal increases mainly the extent of the RWGS reaction, increasing the CO yield. This is well documented by the CO yield curve. After ca. 20 % of the reactor volume, the CO production and consumption start being equilibrated, so that most of the additional CO_2 conversion adds up to the methanol production. In the conditions investigated here, the CO_2 conversion at the reactor outlet is ca. 73 % and the methanol yield is ca. 48 %. The dimensions of the reactor are selected to optimize the space-time yield. An increase of the reactor dimensions could further increase conversion and yield, but the vicinity to the thermodynamic equilibrium would require an excessive volume for a limited increase of reaction yield.

The results here presented generally confirm what is observed in the existing literature [20]. To summarize the results of the entrained flow reactor, the advantage of the continuous operation is compensated by a low selectivity to methanol. This is mainly due to the short contact time in this reactor type, which results in a significant enhancement of the side RWGS reaction. Additionally, the short contact time results in a low catalyst utilization, as a significant amount of catalyst needs to be continuously fed and withdrawn from the reactor. This results in the requirement of a low apparent gas hour space velocity (*GHSV*) to achieve a significant methanol yield. This drawback can be reduced by changing the catalyst utilization, separating the fluid dynamic properties of catalyst and sorbent.

3.3 Entrained and Fluidized Bed Reactor

In the entrained and fluidized bed reactor, the flow pattern of catalyst and sorbent is different. The catalyst is sized to constitute the dense phase in the fluidized bed and hence to remain constantly in the reactor. The sorbent is instead of smaller size, so that it is entrained in the gas flow and continuously fed and withdrawn from the reactor together with the gas. In this way, the main drawback of the entrained flow reactor, i.e., the short residence time of the catalyst in the reactor, is overcome. This reactor type was simulated, and the results are reported in Fig. 5.
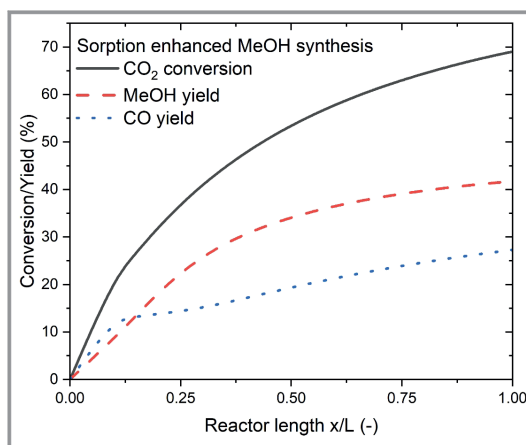

Figure 5. Results of the simulations for the mixed entrained flow/bubbling fluidized bed reactor.

The CO_2 conversion increases continuously over the axial coordinate, until reaching a value of 70 % at the reactor outlet (the outlet conversion value is determined by the reactor size selected). A slight change in the derivative of the CO_2 conversion curve after approximately 10 % of the reactor volume identifies the change of regime from the preferential production of CO to the sorption-enhancement of the methanol synthesis reaction. This is well visible in the methanol and CO yield curves, as in the first 10 % of the reactor volume the main product is CO, while in the rest of the reactor most of the CO_2 is converted to methanol. The positioning of the CO/methanol crossover point and the shape of the CO yield curve are significantly different from the entrained flow reactor. This is mainly due to the different flow pattern, which modifies the relative concentrations of the components and the extent of the competitive reactions and the positioning of the water sorption over the reactor axial coordinate. Overall, the outlet concentrations of CO, CO_2 and methanol are similar to the entrained flow reactor, but the reactor is significantly smaller, thanks to the lower superficial gas velocity at the reactor inlet.

3.4 Comparison of the Reactors

The most appropriate way to compare the performance of the reactors is to consider the variation of methanol yield with the space velocity. This allows determining the dimensions required for a reactor to achieve a certain methanol yield, homogenizing the various properties of the three reactors considered. The comparison is shown in Fig. 6a in terms of *GHSV* and in Fig. 6b considering the amount of catalyst present in the reactor (WHSV, weight hourly space velocity). For the dynamic fixed bed reactor, the calculated space velocity includes the non-reactive residence time due to the sorbent regeneration (e.g., in N_2 flow). One can observe that the fixed bed reactor can reach the highest methanol yield. This is due to the high yield (ideally up to 100 %) achieved with a fresh sorbent, at the reaction start. The cumulative yield decreases quickly with the time on stream, due to the progressive saturation of the sorbent. For this reason, it is not convenient to operate this reactor with *GHSV* higher than 50.

A similar trend is observed in the entrained flow reactor. As already observed in Sect. 3.2, high methanol yield is only achieved with a large reactor. It is also evident that the comparison with the dynamic fixed-bed reactor is unfavorable, as the methanol yield at the same *GHSV* value is lower for the entrained flow reactor. Interestingly, it is also not convenient to operate this reactor at *GHSV* above 50, because the sorption-enhancement effect is practically absent. This is due to the preferential enhancement of the RWGS reaction in the initial stages of the reaction, making the RWGS reaction dominant for high space velocity. The combined entrained flow/fluidized bed reactor also requires a low space velocity to achieve high methanol yield, due to the preferential methanol synthesis mechanism via RWGS and CO hydrogenation. However, due to the different relative extent of these two reactions, with the continuous increase of CO production over the axial coordinate, the methanol yield tends to remain higher at higher space velocity, compared to the other reactors considered. Hence, this reactor type is suitable to achieve larger methanol yield at high space velocity, resulting in a better possibility to manufacture compact units for the methanol synthesis. The main drawback of this reactor type is the significant amount of CO produced, which results in a lower methanol yield also at low *GHSV*. The comparison in terms of *WHSV* shows similar trends. The only exception is that lower *WHSV* is observed for the fixed-bed reactors, because of the low utilization of the catalyst (half of the catalyst is not used because it is in the unit in regeneration.

According to this comparison, we can observe that the dynamic fixed bed reactor is suitable for the production of large amounts of methanol in large units, ideally with quick shift between the reaction and regeneration phase. The entrained/fluidized bed reactor can be a good solution for smaller-scale reactors, where high CO_2 conversion can be achieved in compact units. The drawback of low methanol conversion at large space velocity can be overcome by installing consecutive reaction steps (eventually non-sorption-enhanced) aimed at the conversion of the remaining CO into further methanol. For this reason, a complete comparison of the reactor types should follow the consideration of the reactors in the entire methanol production chain, with the possibility of installing further reactive stages increasing the methanol yield. This optimization problem goes beyond the scope of this study and will be addressed in future research work.
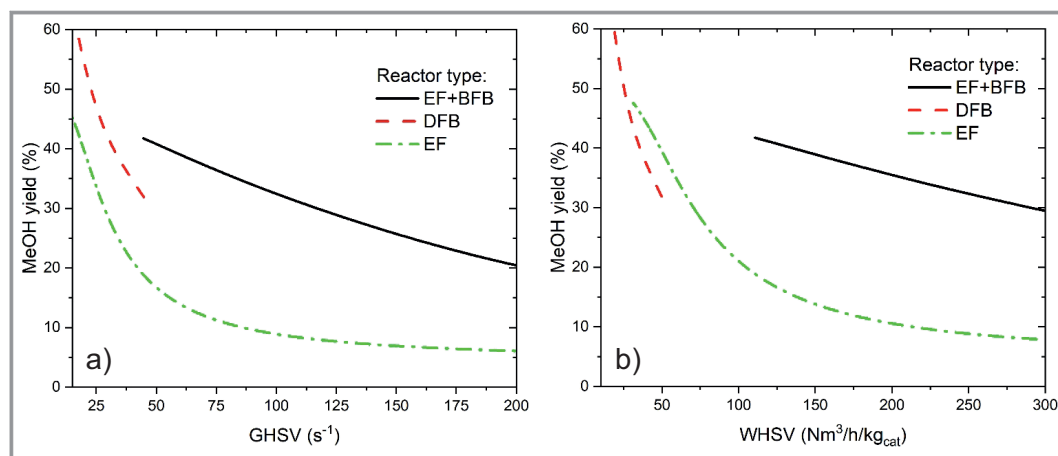

Figure 6. Comparison of the three reactor types: a) methanol yield vs. gas hour space velocity, b) methanol yield vs. weight hour space velocity. The dynamic fixed-bed reactor (DFB) can achieve high methanol yield (> 50 %), but operates at low apparent *GHSV*, due to the relatively high amount of gas required in regeneration. The entrained flow reactor (EF) can achieve high yield only at low space velocity, due to the high superficial velocity required to keep the flow regime. The entrained flow and bubbling fluidized bed reactor (EF+BFB) can achieve significant methanol yield at higher space velocity. The *WHSV* for the DFB is calculated with 150 s of time-on-stream.

4 Conclusion

In this work, we compared the performance of dynamic fixed bed, entrained flow and mixed entrained/bubbling fluidized bed reactors in the sorption-enhanced methanol synthesis. All the reactors are suitable to perform the desired process, but each of them presents pros and cons. The dynamic fixed bed reactor can achieve high methanol yield, thanks to the high utilization of the sorbent (up to the saturation point). However, this reactor is intrinsically discontinuous, as the sorbent must be regenerated. Consequently, the operation requires at least two reactors in series, hence demanding a high amount of catalyst per unit of methanol. The entrained flow reactor achieves a continuous operation of the sorption-enhanced methanol synthesis, but is characterized by a large superficial gas velocity, required to entrain sorbent and catalyst. A better compromise in terms of reactor dimensions and space time yield is achieved by separating the flow pattern of catalyst and sorbent in the reactor, with the former being maintained in the reactor and the latter being entrained. In this case, an adequate methanol yield is achieved also with higher space velocity. However, the methanol selectivity in this reactor is about 60 %, so that further processing of the coproduced CO is required.

The results of this study demonstrate that it is not possible to identify a reactor that clearly shows the best performance in the sorption-enhanced methanol synthesis. The optimal reactor technology strongly depends on external factors, such as required productivity and product purity, availability of heat for the sorbent regeneration and size of the equipment. In fact, these elements influence the number of alternating units required in the dynamic fixed bed reactor operation or the size of the post-processing units to convert CO for all reactor types as well as the size of the sorbent regeneration vessel for the two fluidized bed reactors. In general, it can be observed that the dynamic fixed bed reactor is particularly suitable to produce high amounts of methanol when a fast exchange of the reactive units is possible (i.e., when it is possible to install several units in parallel). The hybrid entrained/fluidized bed reactor could show a better performance for applications that require high CO_2 conversion in a single stage (e.g., small-scale applications), without stringent requirements in terms of methanol yield in a single stage. The decision to apply one specific technology thus depends on the boundary conditions of the system considered. The determination of an optimization routine to select the most suitable technology according to various possible external limitations overcomes the scope of this paper and will be explored in further studies.

Acknowledgments

Appendix

The hydrodynamic parameters for the fluidized bed reactor are as follows:

$$\varepsilon_{mf} = 0.586 \left(\frac{1.0}{Ar}\right)^{0.029} \left(\frac{\rho_g}{\rho_s}\right)^{0.021} \tag{A1}$$

$$U_{mf} = \frac{\mu_g}{\rho_g d_s}\left(\sqrt{25.25^2 + 0.065 \cdot Ar} - 25.25\right) \tag{A2}$$

$$Q_F = U_g^0 A \tag{A3}$$

$$Q_d = U_{mf} A \tag{A4}$$

$$Q_b = Q_F - Q_d \tag{A5}$$

$$d_{bm} = 0.652\left(A\left(U_g^0 - U_{mf}\right)\right)^{0.4} \tag{A6}$$

$$d_{bo} = 0.347\left(7.85\times10^{-5}\left(U_g^o - U_{mf}\right)\right)^{0.4} \tag{A7}$$

$$d_b = d_{bm} - (d_{bm} - d_{bo})\exp\left(-\frac{0.3h}{D}\right) \tag{A8}$$

$$U_b = U_g^o - U_{mf} + 0.711(gd_b)^{0.5} \tag{A9}$$

$$\delta = \frac{U_g^0 - U_{mf}}{U_b} \tag{A10}$$

$$H = \frac{H_{mf}}{1 - \delta} \tag{A11}$$

$$D_{ij} = 0.04357 \frac{T^{2/3}\sqrt{\frac{1}{M_i} + \frac{1}{M_j}}}{P\left(V_{ci}^{1/3} + V_{cj}^{1/3}\right)^2} \tag{A12}$$

$$D_{im} = \frac{1 - x_i}{\sum_{i=1}^{N} \left(\frac{x_i}{D_{ij}} \right)} \tag{A13}$$

$$\frac{1}{(K_{bd})_{ib}} = \frac{1}{(K_{bc})_{ib}} + \frac{1}{(K_{cd})_{ib}} \tag{A14}$$

$$(K_{cd})_{ib} = 6.78 \sqrt{\frac{\varepsilon_{mf} D_{im} U_b}{d_b^3}} \tag{A15}$$

$$(K_{bc})_{ib} = 4.5 \left(\frac{U_{mf}}{d_b} \right) + 5.85 \left(D_{im}^{1/2} g^{1/4} / d_b^{5/4} \right) \tag{A16}$$

$$\frac{1}{(H_{bd})_b} = \frac{1}{(H_{bc})_b} + \frac{1}{(H_{cd})_b} \tag{A17}$$

$$(H_{cd})_b = 6.78 \sqrt{\frac{k_g \rho_g C_{pg} \varepsilon_{mf} U_b}{d_b}} \tag{A18}$$

$$(H_{bc})_b = 4.5 \left(\frac{U_{mf} \rho_g C_{pg}}{d_b} \right) + 5.85 \sqrt{\frac{k_g \rho_g g^{1/2} C_{pg}}{d_b^{5/2}}} \tag{A19}$$

Symbols used

A	[m²]	reactor external surface
A_b	[m²]	surface of a bubble
Ar	[–]	Archimedes number
b_{H_2O}	[Pa⁻¹]	Langmuir adsorption parameter for water adsorption
c_p	[J mol⁻¹K⁻¹]	specific heat
C_D	[–]	drag coefficient
d_s	[m]	diameter of the solids
D	[m²s⁻¹]	diffusion coefficient
F_i	[kmol h⁻¹]	molar flow rate of the species i
Fr	[–]	Froude number
g	[m s⁻²]	gravity acceleration
G_s	[kg m⁻²s⁻¹]	solid circulation rate
H	[m]	reactor length
H_{bd}	[W K⁻¹m⁻²]	heat transfer coefficient from the bubble to the dense phase
ΔH_j^R	[J mol⁻¹]	reaction enthalpy in the reaction j
k	[varies]	apparent kinetic constant
K_{bd}	[mol m⁻²]	mass transfer coefficient from the bubble to the dense phase
n	[–]	apparent reaction order
ΔP	[Pa]	pressure drop
q_{H_2O}	[mol]	water intake of the adsorbent

Q_b	[m³s⁻¹]	volumetric flow rate bubbles
Q_d	[m³s⁻¹]	volumetric flow rate dense phase
r_i	[m]	radius
R	[J mol⁻¹K⁻¹]	universal gas constant
Re	[–]	Reynolds number
S_p	[m²]	particle surface area
t	[s]	time
T	[K]	temperature
T_w	[K]	temperature of the cooling wall
U	[W m⁻²K⁻¹]	heat transfer coefficient
U_g	[m s⁻¹]	gas velocity in the dense region
U_S^0	[m s⁻¹]	superficial solids velocity
v_0	[m s⁻¹]	nitial linear velocity
V_p	[m³]	particle volume
X_i	[–]	conversion of the species i
y_i	[–]	molar fraction
Y_i	[–]	yield of the species i

Greek letters

δ	[–]	bubble phase volume fraction
φ_c	[–]	fraction of the catalyst (among the solids)
ε_b	[–]	bed porosity (considers the void volume in the bed)
ε_{mf}	[–]	solids holdup at minimal fluidization
ε_p	[–]	particle porosity (considers the void volume inside a particle)
ε_s'	[–]	solids holdup when the slip velocity equals U_t
ε_{sd}	[–]	average solids holdup in the dense region
ε_t	[–]	total bed porosity (considers the total void volume $\varepsilon_t = \varepsilon_b + (1 - \varepsilon_b)\varepsilon_p$
η	[–]	catalyst effectiveness factor
$\nu_{i,j}$	[–]	stoichiometric coefficient for species I in the reaction j
ρ_i	[kg m⁻³]	density of the species i
ϕ	[–]	Thiele modulus [-]
ϕ_p	[–]	Sphericity of particles
μ	[Pa s]	dynamic viscosity

References

[1] E. Moioli, *Chem. Eng. Process.* **2022**, *179*, 109097. DOI: https://doi.org/10.1016/j.cep.2022.109097

[2] G. Bozzano, F. Manenti, *Prog. Energy Combust. Sci.* **2016**, 71–105. DOI: https://doi.org/10.1016/j.pecs.2016.06.001

[3] I. U. Din, M. S. Shaharun, M. A. Alotaibi, A. I. Alharthi, A. Naeem, *J. CO2 Util.* **2019**, *34*, 20–33. DOI: https://doi.org/10.1016/j.jcou.2019.05.036

[4] C. Antonini, K. Treyer, A. Streb, M. Van der Spek, C. Bauer, M. Mazzotti, *Sustainable Energy Fuels* **2020**, *4*, 2697–2986. DOI: https://doi.org/10.1039/d0se00222d

[5] E. Moioli, A. Wötzel, T. Schildhauer, *J. Clean. Prod.* **2022**, *359*, 132071. DOI: https://doi.org/10.1016/j.jclepro.2022.132071

[6] K. R. Westerterp, M. Kuczynski, C. H. M. Kamphuis, *Ind. Eng. Chem. Res.* **1989**, *28 (6)*, 763–771. DOI: https://doi.org/10.1021/ie00090a018

[7] R. P. W. J. Struis, S. Stucki, M. Wiedorn, *J. Memb. Sci.* **1996**, *113 (1)*, 93–100. DOI: https://doi.org/10.1016/0376-7388(95)00222-7

[8] J. G. van Bennekom, R. H. Venderbosch, J. G. M. Winkelman, E. Wilbers, D. Assink, K. P. J. Lemmens, H. J. Heeres, *Chem. Eng. Sci.* **2013**, *87*, 204–208. DOI: https://doi.org/10.1016/j.ces.2012.10.013

[9] M. J. Bos, D. W. F. Brilman, *Chem. Eng. J.* **2015**, *278*, 527–532. DOI: https://doi.org/10.1016/j.cej.2014.10.059

[10] J. Reichert, S. Maerten, K. Meltzer, A. Tremel, M. Baldauf, P. Wasserscheid, J. Albert, *Sustain. Energy Fuels* **2019**, *3 (12)*, 3399–3405. DOI: https://doi.org/10.1039/c9se00494g

[11] I. Aloisi, A. Di Giuliano, A. Di Carlo, P. U. Foscolo, C. Courson, K. Gallucci, *Chem. Eng. J.* **2017**, *314*, 570–582. DOI: https://doi.org/10.1016/j.cej.2016.12.014

[12] A. Borgschulte, N. Gallandat, B. Probst, R. Suter, E. Callini, D. Ferri, Y. Arroyo, R. Erni, H. Geerlings, A. Züttel, *Phys. Chem. Chem. Phys.* **2013**, *15 (24)*, 9620–9625. DOI: https://doi.org/10.1039/c3cp51408k

[13] J. Boon, K. Coenen, E. van Dijk, P. Cobden, F. Gallucci, M. van Sint Annaland, *Sorption-Enhanced Water–Gas Shift*, 1st ed., Vol. 51, Elsevier, Amsterdam **2017**.

[14] S. Guffanti, C. G. Visconti, J. van Kampen, J. Boon, G. Groppi, *Chem. Eng. J.* **2021**, *404*, 126573. DOI: https://doi.org/10.1016/j.cej.2020.126573

[15] J. Terreni, M. Trottmann, T. Franken, A. Heel, A. Borgschulte, *Energy Technol.* **2019**, *7 (4)*, 1801093. DOI: https://doi.org/10.1002/ente.201801093

[16] P. Maksimov, A. Laari, V. Ruuskanen, T. Koiranen, J. Ahola, *Chem. Eng. J.* **2021**, *418*, 129290. DOI: https://doi.org/10.1016/j.cej.2021.129290

[17] K. Fujimoto, Y. Yu, *Stud. Surf. Sci. Catal.* **1993**, *77*, 393–396.

[18] J. van Kampen, J. Boon, M. van Sint Annaland, *Adsorption* **2021**, *27 (4)*, 577–589. DOI: https://doi.org/10.1007/s10450-020-00283-8

[19] E. Gabruś, J. Nastaj, P. Tabero, T. Aleksandrzak, *Chem. Eng. J.* **2015**, *259*, 232–242. DOI: https://doi.org/10.1016/j.cej.2014.07.108

[20] M. E. E. Abashar, A. A. Al-Rabiah, *Fuel Process. Technol.* **2018**, *179 (July)*, 387–398. DOI: https://doi.org/10.1016/j.fuproc.2018.07.028

[21] F. Hartig, F. J. Keil, *Ind. Eng. Chem. Res.* **1993**, *32 (3)*, 424–437. DOI: https://doi.org/10.1021/ie00015a005

[22] K. M. Vanden Bussche, G. F. Froment, *J. Catal.* **1996**, *161 (1)*, 1–10. DOI: https://doi.org/10.1006/jcat.1996.0156

[23] F. J. Collado, *Granul. Matter* **2016**, *18 (4)*, 1–14. DOI: https://doi.org/10.1007/s10035-016-0674-5

[24] D. Bai, K. Kato, *Powder Technol.* **1999**, *101*, 183–190.

[25] D. Ba, K. Kato, *J. Chem. Eng. Jpn.* **1995**, *28 (2)*, 179–185. DOI: https://doi.org/10.1252/jcej.28.179

[26] O. . Levenspiel, A. Haider, *Powder Technol.* **1989**, *58*, 63–70.

[27] K. M. Wagialla, H. S. S. E. Elnashaie, *Ind. Eng. Chem. Res.* **1991**, *30*, 2298–2308.

[28] F. Nestler, V. P. Müller, M. Ouda, M. J. Hadrich, A. Schaadt, S. Bajohr, T. Kolb, *React. Chem. Eng.* **2021**, *6 (6)*, 1092–1107. DOI: https://doi.org/10.1039/d1re00071c

[29] L. Spessato, V. A. Duarte, J. M. Fonseca, P. A. Arroyo, V. C. Almeida, *J. CO2 Util.* **2022**, *61 (April)*, 102013. DOI: https://doi.org/10.1016/j.jcou.2022.102013

[30] X. Jiang, X. Nie, X. Guo, C. Song, J. G. Chen, *Chem. Rev.* **2020**, *120*, 7984–8034. DOI: https://doi.org/10.1021/acs.chemrev.9b00723

[31] E. Moioli, T. Schildhauer, *Ind. Eng. Chem. Res.* **2022**, *61 (21)*, 7335–7348. DOI: https://doi.org/10.1021/acs.iecr.1c04682